SMAR 2019 – Fifth Conference on Smart Monitoring,
Assessment and Rehabilitation of Civil Structures

SMAR 2019

Super-resolution images for measuring structural response

Rolands KROMANIS [1], Christopher FORBES [1] and Sushmita BORAH [1]
[1] Nottingham Trent University, Nottingham, United Kingdom

Contact e-mail: rolands.kromanis@ntu.ac.uk

ABSTRACT: Obtaining reliable and precise response measurements of structures subjected to loading is important, especially when assessing their conditions and deriving load-response relationship. A range of contact sensors can collect both structural response and applied loads. When considering beam structures such as girder bridges a control load (a truck of a known weight) can be applied and response can be measured. Developments in digital cameras and image processing enable collection of structural deformations using vision-based technologies, which do not require access to the structure, are non-destructive and low cost. Measurement accuracy largely depends on the image resolution and processing algorithm. When capturing an entire structure in a single image frame, it is unlikely that structural response at multiple locations can be measured accurately. This study proposes to create super-resolution images by stitching high-resolution images, from which accurate structural response is obtained. A robotic camera which is programmed to capture images and rotate along its vertical axis is developed. Initially the accuracy of image stitching is investigated using laboratory beam. The robotic camera captures images at different distances to the structure and zooms. Deformations of a laboratory beam subjected to static loading are then obtained using the robotic camera, smartphone and contact sensors. The results show that the accuracy of measurements collected with the robotic camera system is in a good agreement with the contact sensors and much higher than those obtained with a smartphone camera.

1 INTRODUCTION

Effective monitoring and maintenance of civil structures are important, especially for bridges. Morandi bridge collapse, which took the lives of 43 people, in Italy is a recent example emphasizing the need for a robust bridge monitoring and inspection (O'Reilly et al., 2018). In the UK, general (or visual) bridge inspections are carried out every 24 months (Department for Transport, 2017). Inspections are subjective and depend on inspectors' decisions, which may have human error. Visual inspections are labour intensive and sometimes disruptive (Jahanshahi et al., 2011).

Non-destructive techniques could enhance the general bridge inspection. Contact sensors like accelerometers, strain gauges, linear variable differential transducer (LVDT) are increasingly used in bridge monitoring. Their advantages are limited due to cumbersome and expensive installations and requirements of numerous sensors to monitor structures (Feng and Feng, 2018). Vision-based monitoring systems are non-contact techniques and measure structural response such as deflections. These systems pose promising advantages over contact sensors. For example, vision-based sensors can be found at low-cost, are non-destructive, offer measurement collection of multiple targets, and have a simple instrumentation and installation (Xu and Brownjohn, 2018). Vision-based systems measure displacements of targets (structural features) such as bolts (Feng

and Feng, 2018) when structures are subjected to loading. Structural response such as vertical and horizontal deflections at target locations and strains are measured from displacements of targets (Brownjohn et al., 2017).

Vision-based systems consist of hardware component for image collection and image processing algorithms for calculations of structural response. The response is analyzed for structural performance. Vision-based monitoring systems have been validated in both laboratory experiments and field. For example, Kromanis et al. (2019) have demonstrated the capability of low-cost vision-based systems in various laboratory environments using smartphones. Successful field applications are seen in pedestrian bridges (Feng et al., 2015; Shariati and Schumacher, 2017) and railway bridges (Pan et al., 2016; Ribeiro et al., 2014). The robustness of vision-based systems depends on the quality of the images and the algorithm.

Image quality is sensitive to field conditions like illumination and background disturbance. It is, therefore, pivotal to ensure prudent camera setup to accurately collect image frames, hence improving the quality and output of feature tracking (Feng and Feng, 2016). Super-resolution images (SRIs) are high-quality images that can deliver robust data. The reconstruction of SRIs is the method of producing high-resolution images from a set of low-resolution images (Hu et al., 2009). Brown et al. (2007) indicate the potential of image stitching in creating super-resolution images. Jahanshahi et al. (2011) have used image stitching to reconstruct the stages of damage evolution in a structure and enable inspectors to visually identify damage by comparing stitched current image to the baseline image. Akbar et al. (2019) have demonstrated image stitching to improve the robustness of images taken by unmanned aerial vehicles and identify changes in features. Image stitching may have the potential for monitoring whole structures by capturing the entire structure with a single camera. However, the use of image stitching in vision-based monitoring is mostly confined to feature recognition. Capabilities of feature tracking of structures under load from SRIs have not yet been investigated.

This study proposes to improve the measurement collection accuracy by generating and analysing SRIs. A robotic camera is developed to collect images of parts of the laboratory test-bed. The images are stitched to produce SRIs. SRIs are validated at no load condition by comparing distance between known structural features that are drawn on its surface. The accuracy of the proposed measurement collection technique is analysed by comparing vertical deformations collected by contact sensors and calculated from SRIs, when the test-bed is subjected to known loads.

2 METHODOLOGY

Figure 1 shows a framework of the generation and analysis of SRIs for accurate measurement collection. A robotic camera with a zoom lens captures images of parts of the structure at no load conditions and when the structure is subjected to known loads. Images are stitched generating SRIs, which are then analyzed to obtain structural deformations. The proposed robotic camera system, image stitching and image processing for measuring response are discussed in the subsequent sections.

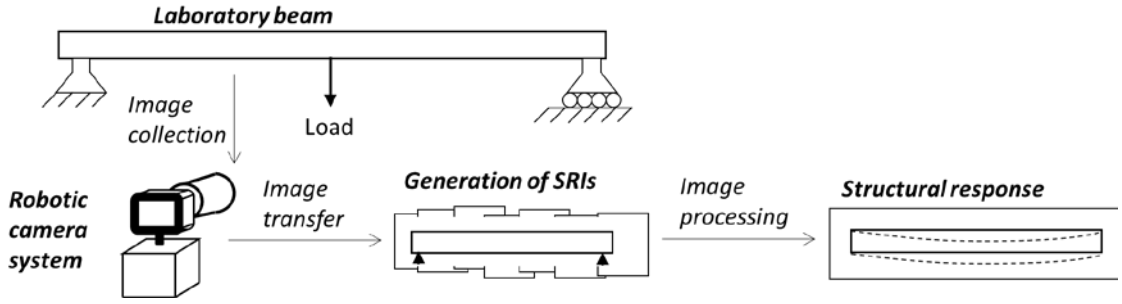

Figure 1. Response measurement collection approach using SRIs.

2.1 Robotic camera development

Images of parts of a structure are needed to generate a SRI of the structure or part of the structure under monitoring. A robotic camera system which rotates the camera, recording visual information of the structure, along its vertical axis is proposed. The camera system can either collect videos or photos. Moving images (from a video) might have motion effect unless collected at a very high frame rate, which in turn, makes video files large and stitching computationally expensive. Therefore, we consider capturing still images instead. After a set of images of a structure is collected, the camera returns to its starting point ready to repeat the cycle.

A prototype for the robotic camera system has been built using a NEMA17 stepper motor fitted with a 5.18:1 ratio gearbox. This is then connected to a laptop via a USB stepper motor controller device. Positioning control is done via a Python script. A GoPro camera that has been custom fitted with a zoom lens is used and controlled via a Wi-Fi connection and Python scripting. Power for the system is supplied from battery packs to allow for portability of the setup. The robotic camera system is then mounted to a standard camera tripod, set to the correct height, and levelled. The robotic camera system works from a single Python script using the steps shown in Figure 2.

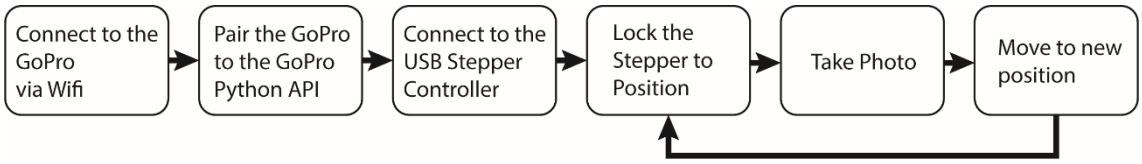

Figure 2. Python Script Steps

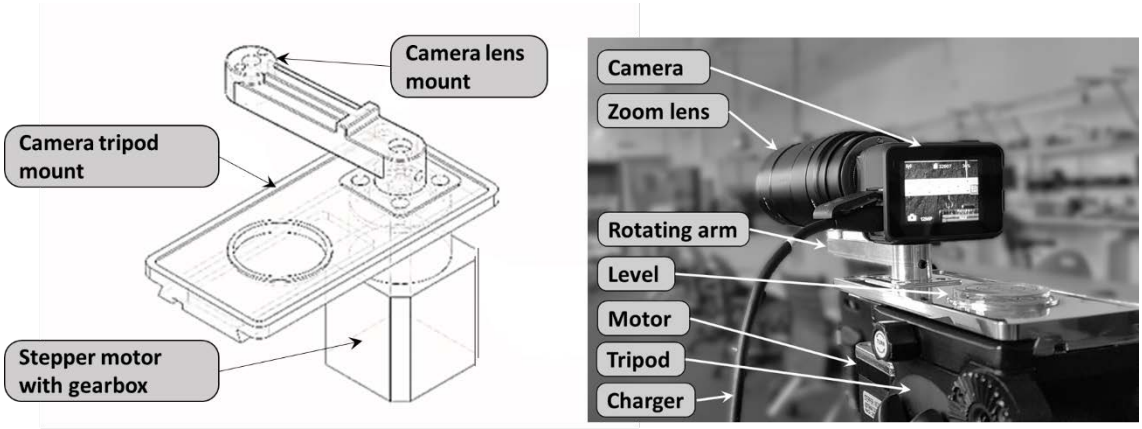

Figure 3. Robotic camera system: model (left) and photo (right).

2.2 Image collection and stitching

The image stitching is the most important part in the generation of SRIs. Each stitched image is recommended to have about 50% image overlap and a sufficient number of common features (Jahanshahi et al., 2011). The main steps involved in image stitching are (in order); image matching, SIFT feature matching, RANSAC homography estimations, bundle adjustment, gain compensation, and multi-band blending. In this study, AutoSitch software developed by (Brown and Lowe, 2007) is employed to generate SRIs.

2.3 Structural deformations

Structural deformations from image frames are extracted when selecting an object of interest or target in a region of interest (ROI). Mathematical features of a target, which are surface features either natural or artificially drawn, are calculated using a suitable feature detection algorithm such as Harris (Harris and Stephens, 2013) for corners. The target is then sought in consecutive images and its location in global image coordinates (x, y) is the arithmetic average of individual feature coordinates. The image coordinates are transformed to a user's defined plane using the planar homography approach (Kromanis and Liang, 2018). Displacements of targets are now available in engineering units.

3 VALIDATION OF IMAGE STITCHING

The image stitching is validated on a timber beam with artificial surface features (blobs or circular objects) drawn on its surface. The setup of the simply supported beam is shown in Figure 4. On both supports a pattern with rectangular shape elements of known dimensions is attached. The coordinates of corners in the pattern are control points for image transformation. Aruco codes are attached to the surface of the beam to aid image stitching. A modified GoPro camera with an adjustable lens of 25 to 135 mm focal length shown in Figure 3 is used in the study. Eight configurations of the robotic camera system ($C_{d,z}$, where d is the camera distance to the beam and z is the focal length of the lens), which are considered for the validation of image stitching, are listed in Table 1. $C_{3m,37mm}$ indicates that the camera system is set 3 m away from the beam and the focal length is 37 mm. In addition to the robotic camera system, a Samsung S9 smartphone, which is set 1 m from the beam, is employed. An image taken with it is shown in Figure 5 (a). Five displacement sensors (Di, where $i = 1,2, \ldots ,5$) are installed above the beam. Displacement values are used in the next section.

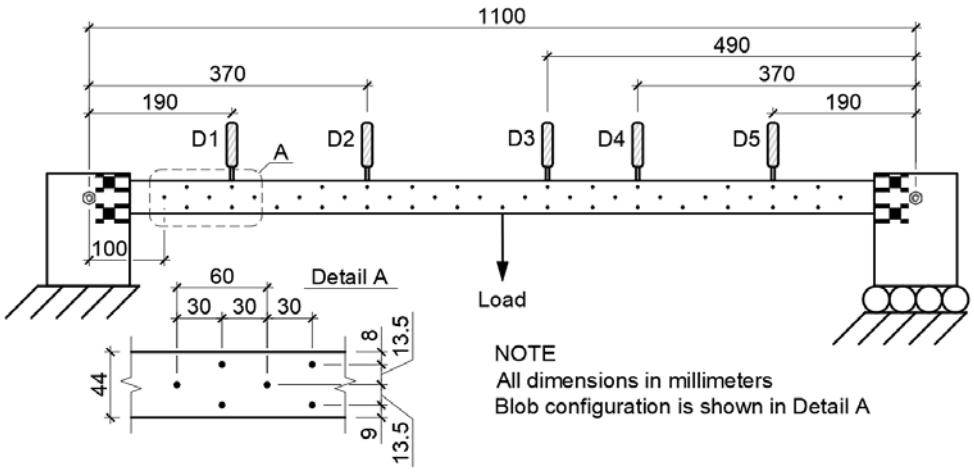

Figure 4. Laboratory test setup.

The steps involved in the evaluation of SRI accuracy are:

- locating and classifying blobs: Blobs are automatically detected and grouped in three rows: top, middle and bottom, according to their location on the beam.
- performing matrix transformation: Transfer blob locations (coordinates) from pixel to real-world units.
- computation of stitching error (e): e is the mean of root mean square errors (RMSEs) between theoretical and calculated distances between two consecutive targets computed for each pair of blobs in each row of blobs.

The number of images captured in a single camera run depends on the selected focal length and the image overlap. Larger the focal length is, larger is the number of images needed to capture the length of the beam. Larger focal length provides more pixels to cover the depth of the beam. Depending on the camera distance to the beam AutoStich offers very high quality stitching. A close view at a part of the beam as captured with $C_{9m,135mm}$ is shown in Figure 5 (d). However, not all images stitched. $C_{3m,115mm}$ and $C_{6m,135mm}$ did not stitch or stitched poorly (see Figure 5 (b)). Blobs are automatically located in SRIs (see Figure 5 (c)). e values for each C scenario are provided in Table 1. The smallest stitching error is when the camera is set 9 m away from the beam.

Blobs are manually drawn on the surface of the beam. Though all measures are taken to achieve high accuracy in the drawing process using a printed template, not all blobs are perfect circles. The drawing error is not considered in this study. It is also very difficult to find the actual center of the blob without considering photogrammetry.

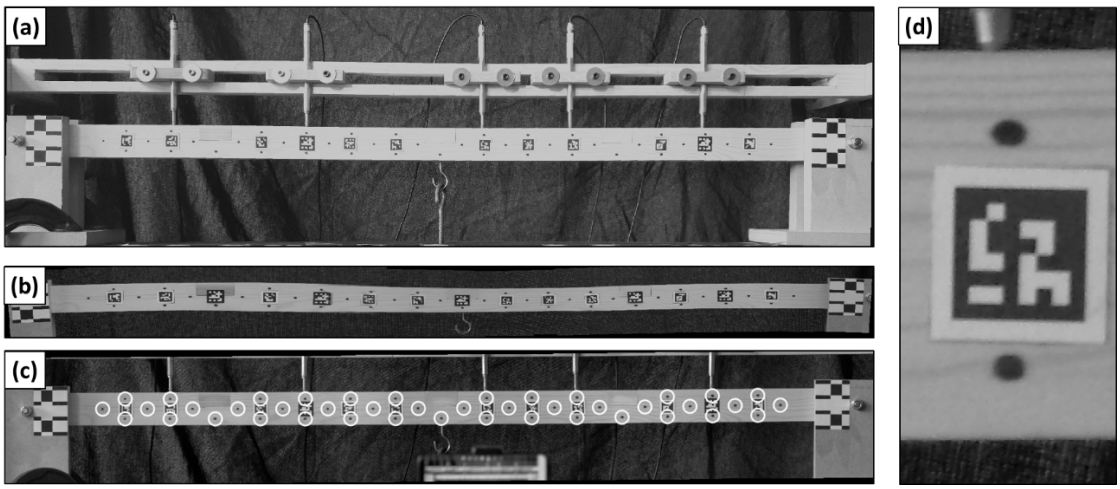

Figure 5. Laboratory setup captured with a smartphone (a). Poorly stitched SRI (b). A SRI with identified blobs (a white circle is drawn around each blob) (c). A close view of a part of the beam with an Aruco code and two blobs (d).

Table 1. Image stitching validation result summary

Camera configuration (C)	Number of images	Image size (px)	Beam depth (px)	Stitching error (e) (px)
Smartphone	1	2268x4032	153	1.15
$C_{3m,37mm}$	8	3012x16101	563	0.21
$C_{3m,86mm}$	14	3164x28115	1020	0.25
$C_{3m,115mm}$	20	Did not stitch	-	-
$C_{6m,74mm}$	6	3206x14117	442	0.10
$C_{6m,98mm}$	14	3292x17968	609	0.12
$C_{6m,135mm}$	21	Did not stitch	-	-
$C_{9m,110mm}$	9	3189x13571	510	0.06
$C_{9m,135mm}$	10	3189x20462	781	0.07

4 EXPERIMENTAL STUDY

The validation of image stitching shows that minimum e is when camera is located 9 m away from the beam. e for $C_{9m,135mm}$ is slightly larger than e for $C_{9m,110mm}$, however the number of pixels covering the depth of the beam is 1.5 times higher for $C_{9m,135mm}$. Therefore $C_{9m,135mm}$ is selected to evaluate the performance of image stitching for accurate measurement collection.

A point load (L_i, where $i = 5N, 15N, 35N, 85N$) is applied at the center of the beam (see Figure 4). A SRI is created at each load. AutoStitch provides limited control over the stitching process, therefore SRIs are not uniform size. Besides, approximately 5 pixel shift is observed after the robotic camera completes a run. These issues require additional image processing steps before deformations at target locations can be measured:

(1) coordinates of the pattern at the left support and the housing of displacement sensors are set as known points. The pattern at the right support is not considered. The right support is anticipated to move left when loads are applied.

(2) the points are located in each SRI and then used to generate a transformation matrix.

(3) coordinates of five targets, blobs under sensor locations, are extracted from SRIs and transformed to the coordinate system defined in step (2). Targets (Ti, where $i = 1,2, \dots ,5$) are named according to displacement sensor (D) locations (see Figure 3).

Locations of targets in both images collected with smartphone and SRIs during the load test are obtained using DeforMonit (Kromanis et al., 2019). A user specifies a ROI in which a target is located. The location of the target is computed as follows: (i) convert the image with ROI from color to grayscale, (ii) adjust image (sharpen, brighten, increase size), (iii) convert adjusted image to a binary image (black and white), (iv) draw the best fit ellipse around the blob (v) and output coordinates of the center of the ellipse. As an example, vertical deflections at D2 location obtained with all measurement collection approaches at four loads are given in Figure 6 (left). RMSE between robotic camera and displacement sensors and smartphone and displacement sensors are plotted in Figure 6 (right). RMSE values confirm that the proposed measurement collection approach using SRIs outperforms the conventional vision-based measurement collection approach.

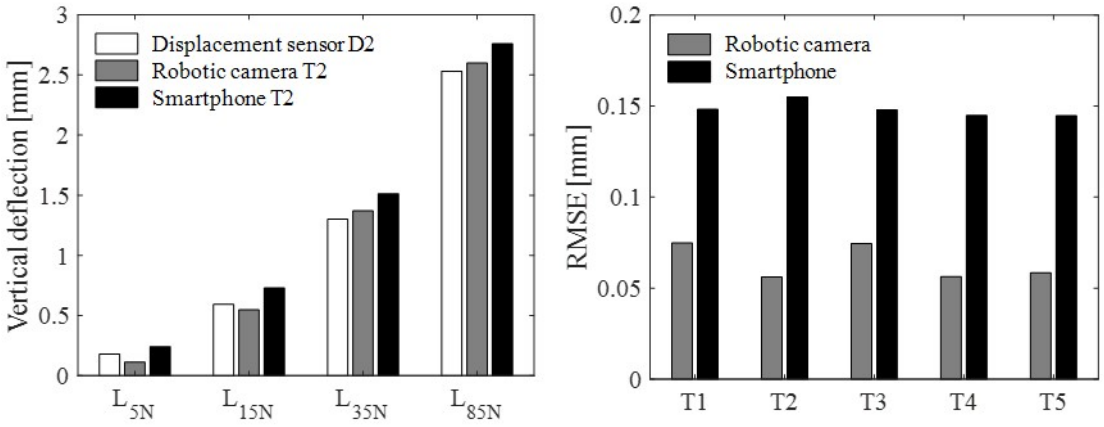

Figure 6. Vertical deflection at D2 location (left) and RMSE between vision-based technologies and contact sensors.

4.1 Discussion

The robustness of the proposed approach relies on accuracy of (a) the robotic camera, (b) image stitching, (c) target tracking, and (d) planar homography. The camera rotation error requires adjustments of calculated target locations, which is made more complicated, when detecting that consecutively captured SRIs have a slight stitching error. This can be fixed following the steps provided in this section, however, ideally such errors should not occur. Measurement errors could be reduced by improving or changing the image stitching technique. The technique could be tailored to specific task such as stitch images horizontally and refer to the first SRI image.

5 CONCLUSIONS

This study introduces a new approach for collecting accurate structural deformations using super-resolution images (SRIs). A robotic camera captures still images of parts of the structure at no load and subjected to static loads. Images are stitched creating SRIs, which are analyzed with image processing tools to obtain high accuracy structural response. This study draws the following conclusions:

- Overall the developed robotic camera system shown in Figure 3 performs well. The robotic camera has a small rotation error, which is around 5 pixels, when the camera is set 9 m away from the beam.
- Accurate SRIs can be created using AutoStitch application. However the control over the image stitching process is limited resulting in stitching errors when generating SRIs.
- Structural response at target locations computed using the proposed image stitching approach with SRIs is more accurate in comparison to the response collected from a single image frame.

Freeware (open source software) such as DeforMonit (employed in this study) can be used to obtain reliable deformations of structures. Their availability and capability to measure accurately deformations of structures make them an attractive alternative to commercial software. Besides, SRIs offer even higher level of accuracy in comparison to single frame images. The superior quality of images generated with a robotic camera system can provide useful information of the material surface, which, for example, could be analyzed for cracks in steel and concrete structures.

6 REFERENCES

Akbar, M.A., Qidwai, U., Jahanshahi, M.R., 2019, An evaluation of image-based structural health monitoring using integrated unmanned aerial vehicle platform. *Structural Control and Health Monitoring*, 26, 1–20.

Brown, M., Lowe, D.G., 2007, Automatic panoramic image stitching using invariant features. *International Journal of Computer Vision*, 74, 59–73.

Brownjohn, J.M.W., Xu, Y., Hester, D., 2017, Vision-Based Bridge Deformation Monitoring. *Frontiers in Built Environment*, 3, 23.

Department for Transport, 2017, Inspection of highway structures, Design Manual for Roads and Bridges.

Feng, D., Feng, M.Q., 2016, Vision-based multipoint displacement measurement for structural health monitoring. *Structural Control and Health Monitoring*, 61, 215–223.

Feng, D., Feng, M.Q., 2018, Computer vision for SHM of civil infrastructure: From dynamic response measurement to damage detection – A review. *Engineering Structures*, 156, 105–117.

Feng, D., Feng, M.Q., Ozer, E., Fukuda, Y., 2015, A vision-based sensor for noncontact structural displacement measurement. *Sensors (Switzerland)*, 15, 16557–16575.

Harris, C., Stephens, M., 2013, A Combined Corner and Edge Detector. In: Alvey Vision Conference. pp. 147–151.

Hu, Y., Ning, B., Li, X., Gao, X., Tao, D., 2009, A multi-frame image super-resolution method. *Signal Processing*, 90, 405–414.

Jahanshahi, M.R., Masri, S.F., Sukhatme, G.S., 2011, Multi-image stitching and scene reconstruction for evaluating defect evolution in structures. *Structural Health Monitoring*, 10, 643–657.

Kromanis, R., Liang, H., 2018, Condition assessment of structures using smartphones : a position independent multi-epoch imaging approach. In: 9th European Workshop on Structural Health Monitoring, July 10-13, 2018, Manchester, UK. Manchester, pp. 1–10.

Kromanis, R., Yan, X., Lydon, D., Rincon, J.M. del, Al-Habaibeh, A., 2019, Measuring structural deformations in the laboratory environment using smartphones. *Frontiers in Built Environment*, 5.

O'Reilly, G.J., Monteiro, R., Scattarreggia, N., Martino Calvi, P., Pinho, R., Calvi, G.M., Malomo, D., Moratti, M., 2018, Once upon a Time in Italy: The Tale of the Morandi Bridge. *Structural Engineering International*, 0, 1–20.

Pan, B., Tian, L., Song, X., 2016, Real-time, non-contact and targetless measurement of vertical deflection of bridges using off-axis digital image correlation. *NDT and E International*, 79, 73–80.

Ribeiro, D., Calçada, R., Ferreira, J., Martins, T., 2014, Non-contact measurement of the dynamic displacement of railway bridges using an advanced video-based system. *Engineering Structures*, 75, 164–180.

Shariati, A., Schumacher, T., 2017, Eulerian-based virtual visual sensors to measure dynamic displacements of structures. *Structural Control and Health Monitoring*, 24, 1–9.

Xu, Y., Brownjohn, J.M.W., 2018, Review of machine-vision based methodologies for displacement measurement in civil structures. *Journal of Civil Structural Health Monitoring*, 8, 91–110.